Condensed Matter Physics 2007, Vol. 10, No 1(49), pp. 51–60

Electret effect in intercalated crystals of the $A^{III}B^{VI}$ group

I.Grygorchak[1], S.Voitovych[1], I.Stasyuk[2], O.Velychko[2], O.Menchyshyn[2]

[1] Lviv Polytechnic National University, 12 Bandera Str., 79013 Lviv, Ukraine
[2] Institute for Condensed Matter Physics of the National Academy of Sciences of Ukraine, 1 Svientsitskii Str., 79011 Lviv, Ukraine

Received January 25, 2007

Measurements of dielectric properties of Ni-intercalated GaSe and InSe have been performed. The present study is aimed at the investigation of the low-admixture region where the intercalation induced electret effect occurs. The effect exhibits pronounced peak-like concentration dependences and a non-monotonous temperature behaviour with maximum magnitudes at low temperatures. Intercalation leads to over tenfold increase of dielectric permittivity over the whole measured frequency range with up to several orders at low frequencies for GaSe. Temperature dependences of the permittivity demonstrate well-defined peaks with localizations and heights strongly depending on the concentration. A microscopic model of order-disorder type has been proposed that considers redistribution of intercalant atoms between non-polar octahedral and polar tetrahedral positions in the crystal van der Waals gaps. Such a redistribution can occur in the form of phase transition to the polar phase (corresponding to the electret effect) which is stabilized by the internal field. For the case of octahedral positions being more preferable, the model predicts a peak-like dependence of the crystal polarization on chemical potential due to passing through the interjacent polar phase in accordance with the measured behaviour of the electret effect. The calculated temperature dependences of dielectric susceptibility qualitatively reproduce experimental results for permittivity as well.

Key words: *monochalcogenides, electrets, intercalation, lattice gas model*

PACS: *71.20.Tx, 77.22.Ej, 71.10.-w, 05.50.+q*

1. Introduction

There are eleven chalcogenides of the $\mathrm{A^{III}B^{VI}}$ type [1–4]: AlS is unstable in ambient air, BS exists only in gaseous state and nine others are stable solids. These compounds are divided into three subgroups with different crystal structures: a gallium sulphide type (GaS, GaSe, GaTe, InS, InSe), a thallium sulphide type (TlS, TlSe, InSe) and thallium telluride as a solitary type. A special feature of the gallium sulphide subgroup is a layered crystal structure. Each layer consists of four sublayers BAAB (A = Ga, In; B = S, Se, Te) with atoms arranged in a hexagonal close packing. Every metal atom A has a tetrahedral sp^3 coordination formed by three B atoms and another A atom, and every chalcogen atom B has a pyramidal p^3 coordination with a filled s^2 shell. Bonds between A and B are covalent with some ionic character while the interaction of A atoms is pure covalent. These complex layers are bound together by a weak van der Waals interaction (in a way similar to the molecular crystals).

There are four possible stacking arrangements of complex layers leading to four polytypes designated β, ε, γ and δ. Three of these polytypes (β, ε, γ) are usually observed in grown monocrystals, the δ-polytype being found in the powder phase only. The β-polytype corresponds to a rotation by π around the axis perpendicular to the plane of the layer followed by a translation parallel to the axis of rotation; the other two ways correspond to a translation where the horizontal components are $-(\mathbf{a}_1+\mathbf{a}_2)/3$ in one case (ε-polytype) and $(\mathbf{a}_1+\mathbf{a}_2)/3$ in the other case (γ-polytype). The $\mathbf{a}_i$ are basis vectors of a hexagonal lattice.

The ε-polytype has a hexagonal close packing. An elementary cell consists of two translationally nonequivalent layered packs (A$\updownarrow\updownarrow$A) and (B$\bigcirc\bigcirc$B) with space group D^1_{3h}. The crystal structure of the β-polytype (space group D_{6h}^4) has an inversion centre unlike the previous one; lattice constants for both the polytypes are identical. Two alternative choices of the unit cell are considered for the γ-polytype having the third translationally nonequivalent layered pack (C$\mapsto\mapsto$C): the rhombohedral primitive unit cell extending over one layer (2A and 2B atoms) or the hexagonal extended unit cell spanning over three layers (space group C_{3v}^5).

During the intercalation, the impurity atoms enter the mentioned van der Waals gaps between the layers. There are three interstitial sites per formula unit available in the gap (figure 1): one octahedral (surrounded by six chalcogen atoms) and two tetrahedral (lying in the projections below and above the chalcogen atoms). The octahedral site is located in the middle of the gap while tetrahedral sites are symmetrically shifted towards the top and the bottom layers, respectively.

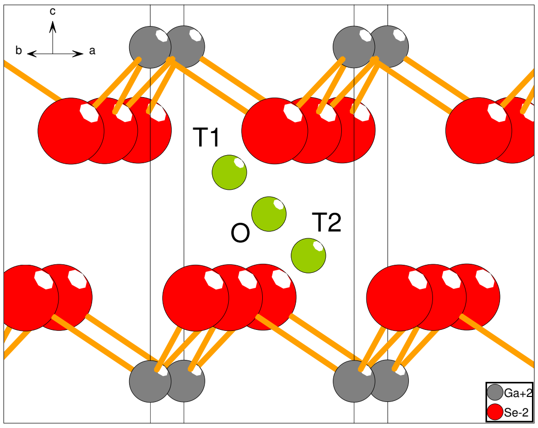

Figure 1. Octahedral (O) and tetrahedral (T1, T2) sites for intercalated particles in a van der Waals gap of the GaSe crystal.

Ba or Li intercalated indium selenide may be applied as solid solution electrodes, in particular in those cases where intercalation is possible over a wide stoichiometry range. For this reason InSe is a good candidate for intercalation electrodes. Its photoconductive behaviour and photomemory effect [5,6] permit the design of a dual device: a secondary battery combined with a photovoltaic system. The relation between photoelectric processes and electret effect in the Li-intercalated gallium and indium selenides was studied in work [7]. Measurements of temperature dependences of resistivity and dielectric susceptibility (both perpendicular to the layers) as well as spectral dependences of photocurrent for ferroelectric ($NaNO_2$, KNO_2) intercalated gallium and indium selenides reveal their cardinal changes due to intercalation [8]. There are some differences in the behaviour of resistivity perpendicularly to the layers during the intercalation by Li: in GaSe it rises 10^4 times but in InSe it first falls $3 \cdot 10^2$ times and then rises $3 \cdot 10^3$ times [9]. It was also established that intercalation of GaSe causes the narrowing of the frequency-independent region of resistivity and makes it more temperature dependent. Intercalation neither changes the symmetry of the crystals nor the in-plane lattice constant a, whereas the constant c (perpendicular to the planes) slightly increases. Similar measurements of resistivity temperature dependences were performed for the β-polytype of InSe single crystals of p- and n-type intercalated with Ba and Li by electrochemical process [10]. A decrease of resistivity for n-InSe and its increase for p-InSe were observed with respect to non-intercalated samples.

A number of theoretical *ab initio* calculations have been made for pure and intercalated layered crystals of the GaS type. The first band structure calculations were performed for pure GaSe [11] and InSe in two- [12] and three-dimensional cases [13,14]. The diffusion path of the intercalated Li atoms in InSe was studied by means of total energy calculation [15]. A study of the electronic energy bands and lattice dynamics of pure and Li-intercalated InSe based on electronic energy band calculations established that the intercalated sample had an impurity band just below the conduction band edge [16,17]. Baric dependences of the pure InSe crystal structure as well as the phonon frequencies in the pressure range up to 15 GPa were calculated [18]. A better insight into the physical mechanism of intercalation induced phenomena can be achieved employing the models of the lattice gas type [19]. Such models are usually formulated in more general manner or can be more specific taking into account the peculiar features of the system considered. For example, the study of InSe and GaSe intercalated by alkali metals within the framework of the lattice gas model [20] revealed large deformation strains in the intercalated hosts. A similar approach implying the existence of a link between the elastic properties of the host material and the structure and dynamics associated with the guest species has been developed for two- [21] as well as for three-dimensional systems [22,23]. The model is general enough to describe various non-isomorphous intercalated systems (layered Li_xTiS_2, crystalline Li_xWO_3, Na_xWO_3, Li-graphite) providing a good agreement with the experiment despite the fact that some specific structure data are omitted. However, neglecting the crystal structure peculiarities (e.g. more than one position for the intercalated particle per formula unit) prevents this model from describing a class of effects that include the electret one. Even the model [24] considering octahedral and tetrahedral positions in van der Waals gaps of GaS-type crystals without proper account of interactions between the particles in these positions is incapable of solving the problem due to the collective nature of an order-disorder phenomenon such as the electret effect. These interactions and order-disorder transitions were considered in work [25] where a model of the Blume-Emery-Griffiths (BEG) type was investigated. Unfortunately, this model took only tetrahedral positions into account. Thus the model of choice should incorporate a necessary structure information as well as a long-range nature of interactions preserving at the same time as much simplicity and generality as possible.

The present study concerns the electret effect as another unusual phenomenon induced by intercalation in gallium and indium selenides. Temperature and concentrational dependences of the dielectric properties for intercalated crystals are presented. A credible origin of the phenomenon is described by a microscopic four-state model capable of reproducing the peculiarities of thermodynamic behaviour for the compounds investigated.

2. Manifestations of the electret effect in GaSe and InSe crystals

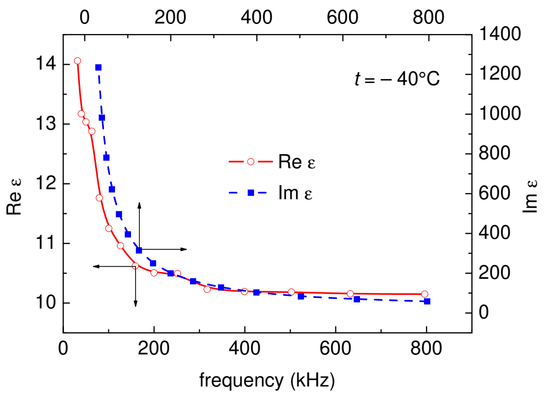

Figure 2. Real and imaginary parts of permittivity of pure GaSe illustrating fulfilment of the "universal dielectric response" law.

The term "electret effect" will be taken here to mean a polar state leading to a non-zero voltage between the surfaces of the crystal in the direction of the crystallographic *c*-axis i.e. perpendicular to the planes. Electrets are widely used in industry for production of microphones, hydrophones, electrophotography, pyroelectric videcons, electret filters, electromechanical transformers, electret motors, dosimeters etc. A novel type of intercalated electrets has a lot of prominent features. Their resistivity is three to four orders lower compared to usual electrets which ensures better power characteristics of respective devices. A wide low-temperature region of thermodepolarization makes it possible to use these compounds for low-temperature solid state power generators [26] with simultaneous accumulation of the solar energy converted *in situ* to the electric one. The maximum value of photoelectric EMF is two times higher compared to the known semiconductive photocells. Electret voltage of the intercalated compounds strongly depends on the value of ambient pressure making them sensitive tensometric transducers for direct measurements of low hydrostatic pressure with high-intensity output electric signal without amplification [27]. Intercalated electrets have also got abnormally high values of dielectric permittivity which is very sensitive to the external electric field. So, these compounds can be used for a new generation of variconds with ten times higher specific capacity and control coefficients [28].

Intercalation induced electret effect was observed for the first time in the intercalated GaSe [29]. The crystals were intercalated by Li, Na and K. The value and the sign (positive for Li, Na and negative for K) of the voltage depend on concentration and type of intercalant. The effect was quite stable, the best durability (about a year) was obtained for Li intercalation; it decreased with rise of the intercalant atomic number. Maximum values of the thermostimulated discharge current were observed at intercalant concentration of 10^{18}–10^{19} cm^{-1}. The increase of the intercalant atomic

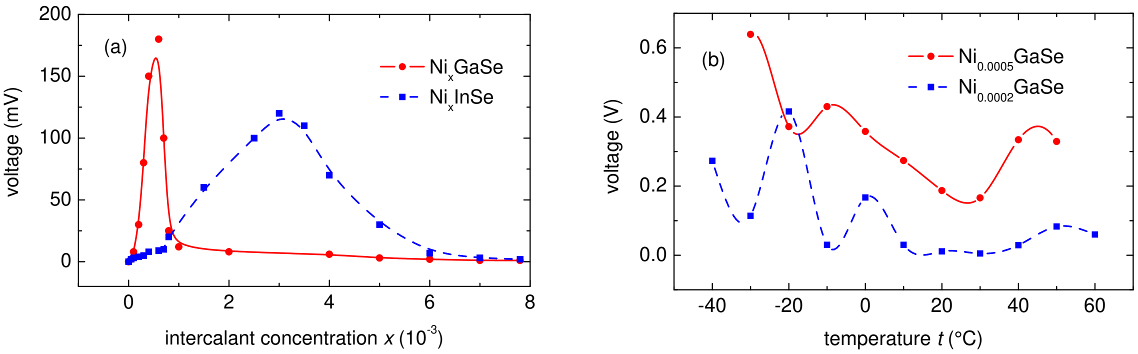

Figure 3. Dependences of the electret effect magnitude: (a) on the intercalant concentration for Ni_xGaSe and Ni_xInSe crystals measured at room temperature and (b) on temperature for Ni_xGaSe at various intercalant concentrations.

number shifts the peaks of the corresponding temperature dependences of the current to lower temperatures and decreases their maximum values. The magnitudes of thermostimulated current in the Li and Na intercalated GaSe significantly decrease after the first run of temperature cycling but remain almost stable during the following runs. Such a behaviour is presumably related to the formation of the quasidipoles oriented in one direction that are induced by intercalant cations.

The crystals studied in the present work were grown using the Bridgman-Stockbarger method in the quartz vacuum-sealed ampoules. The measurements of the crystal low-frequency (20 Hz–800 kHz) dielectric spectrum (figure 2) demonstrate a "classic" behaviour and obeys the Jonscher's power law. Both surfaces (parallel to the layers) of the crystals were equipotential in the whole temperature region (from -40°C to $+60$°C) before intercalation. A pronounced electret effect is observed after intercalation in a rather narrow region of intercalant concentrations, especially for gallium selenide (figure 3(a)). Temperature dependences of electret effect magnitude (figure 3(b)) demonstrate a complicated non-monotonous behaviour with noticeable shift of higher values of magnitudes to the low-temperature segment. The maximum value of the magnitude (3.89 V at -40°C for $Ni_{0.0005}$GaSe) coincides with the singular point of the thermal resistivity coefficient perpendicular to the layer which is presumably related to "softening" of the phonon spectrum.

The dielectric spectrum of the crystals was measured by the impedance spectroscopy method using Eco Chemie B.V. (the Netherlands) "Autolab" equipment with the FRA-2 and GPES software. Intercalation leads to over tenfold increase of dielectric permittivity (figure 4) over the whole frequency range (10^{-3}–10^{6} Hz) with a dramatic magnitude growth (up to several orders depending on the Ni concentration) at low frequencies (up to 100 Hz) for Ni_xGaSe (figure 4(a)).

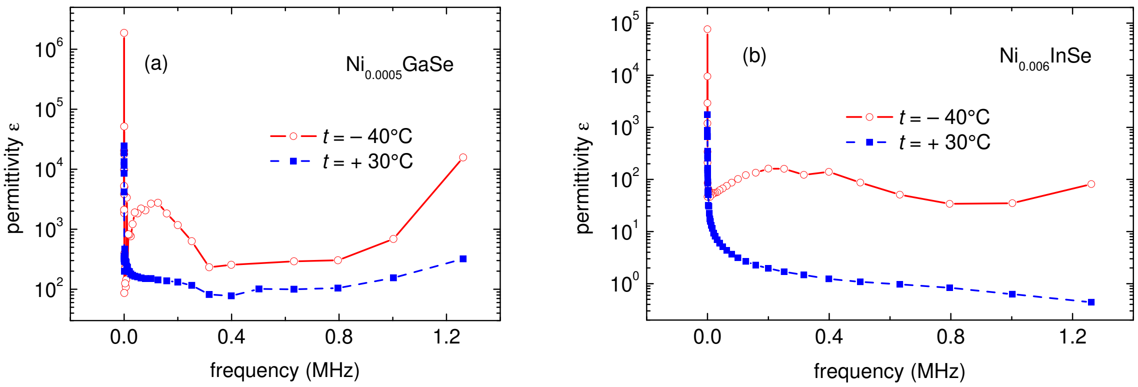

Figure 4. Frequency dependences of the real part of the dielectric permittivity for (a) $Ni_{0.0005}$GaSe and (b) $Ni_{0.006}$InSe measured at various temperatures.

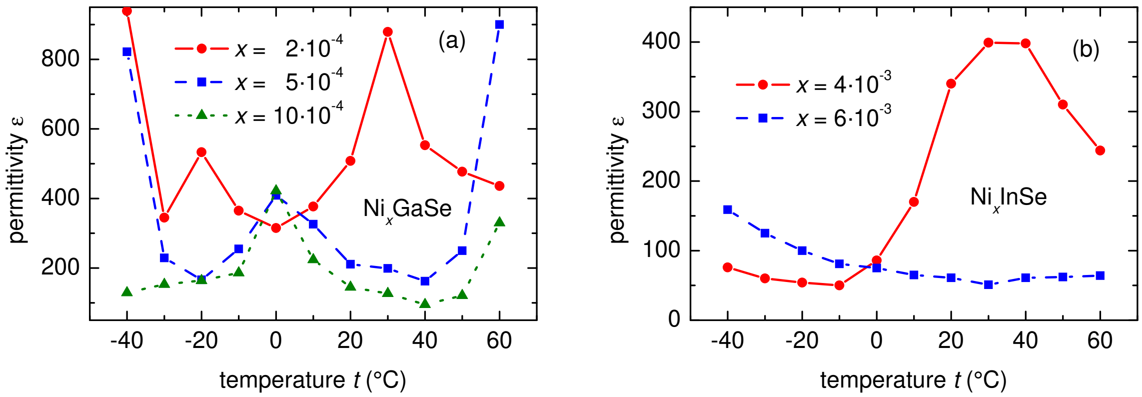

Figure 5. Temperature dependences of the real part of the dielectric permittivity measured at various intercalant concentrations for (a) Ni_xGaSe and (b) Ni_xInSe crystals.

The observed frequency dispersion is of abnormal character with a pronounced temperature dependence. According to the classical theory, the real part of dielectric permittivity should not increase with the rise of frequency. The only exception is a high-frequency (optical range) resonance polarization in some materials [30]. In such a case non-monotonous behaviour of dielectric permittivity is caused by the jump-like charge transfer between the defects with a neutral ground state. This charge transfer produces effective dipoles leading to additional polarization with dispersion given by the expression [31]: $\chi \propto \nu^{-(\alpha+2)}$, where ν is the frequency. At $\alpha < -2$ this dispersion becomes abnormal.

Taking into account the above considerations, temperature dependence of the dielectric permittivity was measured for its low-frequency normal branch of frequency dispersion with the tangent of the losses angle in the range 0.01–0.4. Temperature dependences of permittivity demonstrate well-defined peaks with localization strongly depending on the Ni concentration (its increase shifts maxima to the low-temperature region) (figure 5(a)). Crucial effect of concentration change on the peak-like behaviour of the permittivity is especially noticeable in the Ni_xInSe intercalated compound with smaller width of the energy gap, where the peak completely disappears at the increase of concentration from 0.004 to 0.006 (figure 5(b)). The presence of the permittivity peak indicates that the system is close to the state of dielectric instability.

3. Theoretical description of the electret effect by the extended model of the lattice gas type

To describe the intercalant subsystem in the considered crystals we propose a four-state generalization of the $S = 1$ BEG model [32,33]. Empty sites in the unit cell are denoted as state "1". Localization of the intercalant particle in the top or in the bottom tetrahedral position corresponds to the states "2" or "4" having energy E' while the occupation of the octahedral position corresponds to the state "3" having energy E. We suppose that only one position in the unit cell can be occupied at a time. So the system is characterized by the polarization order parameter $\sigma = \langle X^{22}\rangle - \langle X^{44}\rangle$ as well as by occupations of tetrahedral (polar) $n = \langle X^{22}\rangle + \langle X^{44}\rangle$ and octahedral (non-polar) $n' = \langle X^{33}\rangle$ positions, respectively, where $X^{\alpha\alpha}$ are projection operators. Further we use the half-sum $\varepsilon_0 = (E + E')/2$ and the half-difference $\Delta = (E - E')/2$ of the position energies.

In the model Hamiltonian we take into account the effective field $h = dE$ (where d is the effective dipole moment and E is the field strength) acting on the polar states in the transverse direction (perpendicularly to the layers) and assume that interaction between the particles depends on their local positions:

$$H = H_0 + H',$$

$$
\begin{aligned}
H_0 &= \sum_i \left[E X_i^{33} + E'(X_i^{22} + X_i^{44})\right] - \mu \sum_i \left[X_i^{22} + X_i^{33} + X_i^{44}\right] - h \sum_i \left[X_i^{22} - X_i^{44}\right], \\
H' &= -\frac{1}{2} \sum_{ij} \sum_{\alpha\beta} W_{ij}^{\alpha\beta} X_i^{\alpha\alpha} X_j^{\beta\beta}.
\end{aligned} \tag{1}
$$

The effective field h (or E) is a superposition of the external electric field (if present) and the internal electric field produced by redistribution of intrinsic charged impurities or defects as well as current carriers in the crystals (under the action of intercalant atoms in van der Waals gaps).

In the mean field approximation the interaction part is as follows

$$
\begin{aligned}
H'_{\text{MFA}} = {} & \frac{N}{2}\left[Vn^2 + J\sigma^2 + 2Unn' + (V+J)n'^2\right] - \sum_i \left[Vn + J\sigma + Un'\right] X_i^{22} \\
& - \sum_i \left[Un + (V+J)n'\right] X_i^{33} - \sum_i \left[Vn - J\sigma + Un'\right] X_i^{44},
\end{aligned} \tag{2}
$$

where $V = \frac{1}{2}(W_{22}+W_{24})$, $U = W_{23} = W_{34}$, $J = \frac{1}{2}(W_{22}-W_{24})$ and $W_{\alpha\beta} = W^{\alpha\beta}(0)$ are the Fourier transforms of corresponding interaction energies taken in the center of the Brillouin zone. Next a set of self-consistency equations for polarization as well as occupancies of polar and nonpolar states was derived:

$$
\left\{
\begin{aligned}
\sigma &= 2\sinh\beta(J\sigma + h)\exp\left[-\beta(\varepsilon_0 - \mu - \Delta - Vn - Un')\right]/Z \\
n &= 2\cosh\beta(J\sigma + h)\exp\left[-\beta(\varepsilon_0 - \mu - \Delta - Vn - Un')\right]/Z \\
n' &= \exp\left[-\beta(\varepsilon_0 - \mu + \Delta - Un - (V+J)n')\right]/Z
\end{aligned}
\right. , \tag{3}
$$

$$
\begin{aligned}
Z = {} & 1 + 2\cosh\beta(J\sigma + h)\exp\left[-\beta(\varepsilon_0 - \mu - \Delta - Vn - Un')\right] \\
& + \exp\left[-\beta(\varepsilon_0 - \mu + \Delta - Un - (V+J)n')\right].
\end{aligned}
$$

Thermodynamically stable solutions of the above set are chosen based on the criterion of the minimal value of the grand canonical potential:

$$
\Omega/N = \frac{1}{2}\left[Vn^2 + J\sigma^2 + 2Unn' + (V+J)n'^2\right] - \Theta \ln Z. \tag{4}
$$

There are four possible phases in the ground state: empty sites, octahedral positions occupied (both with zero polarization) and tetrahedral positions occupied (positive or negative polarization):

1. $\sigma = 0$, $n = 0$, $n' = 0$, $\lambda_1 = 0$, $\Omega_1/N = 0$.
2. $\sigma = 1$, $n = 1$, $n' = 0$, $\lambda_2 = \varepsilon_0 - \mu - \Delta - V - J - h$, $\Omega_2/N = \varepsilon_0 - \mu - \Delta - (V+J)/2 - h$.

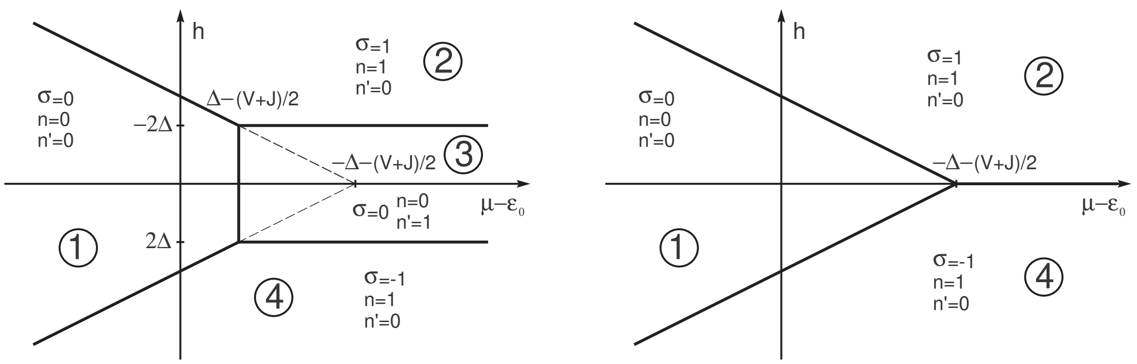

Figure 6. The phase diagrams of the ground state for the case $\Delta < 0$ (left) and the case $\Delta > 0$ (right) in the "chemical potential – effective field" plane.

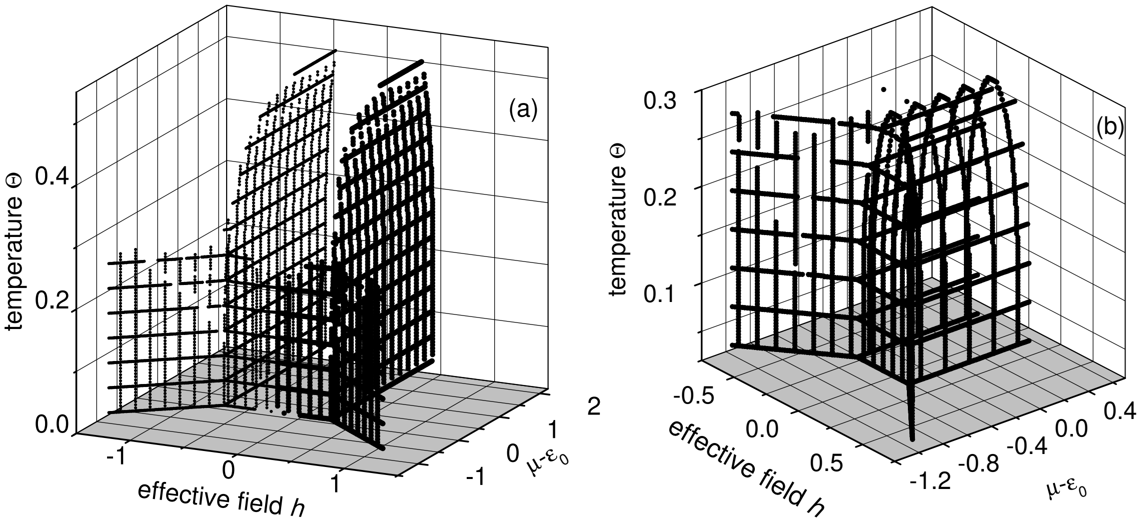

Figure 7. Surfaces of phase transitions separating phases for the case $\Delta < 0$ at $V = 1$, $J = 0$, $U = 0$; (a) $\Delta = -0.25$ and (b) $\Delta = -0.1$, respectively.

3. $\sigma = 0,\ n = 0,\ n' = 1,\ \lambda_3 = \varepsilon_0 - \mu + \Delta - (V + J),\ \Omega_3/N = \varepsilon_0 - \mu + \Delta - (V + J)/2.$

4. $\sigma = -1,\ n = 1,\ n' = 0,\ \lambda_4 = \varepsilon_0 - \mu - \Delta - V - J + h,\ \Omega_4/N = \varepsilon_0 - \mu - \Delta - (V + J)/2 + h.$

The knowledge of grand canonical potentials for each phase allows us to build the phase diagram (figure 6). The most interesting case appears for negative values of the energy half-difference Δ. The increase of the chemical potential stimulates the occupation of sites by the intercalant and the effective field makes polar states more preferable. The nonpolar occupied phase “3” is located between the polar phases at small values of the field. In the case of positive values of the energy half-difference Δ this occupied nonpolar state is completely suppressed in the ground state and the phase diagram closely resembles the $S = 1$ Blume-Emery-Griffiths one. However, in the general case the shape of the phase diagram depends on temperature: lines of phase transitions are shifted and deformed until the transitions completely vanish at high enough temperatures (figure 7; hereinafter all interaction parameters, temperature, chemical potential and the effective field h presented in figures are normalized by the sum $V + J$).

At certain values of the model parameters and temperature there is a possibility to pass sequentially through three phases “1–2–3” at the increase of chemical potential (figure 8(a)).

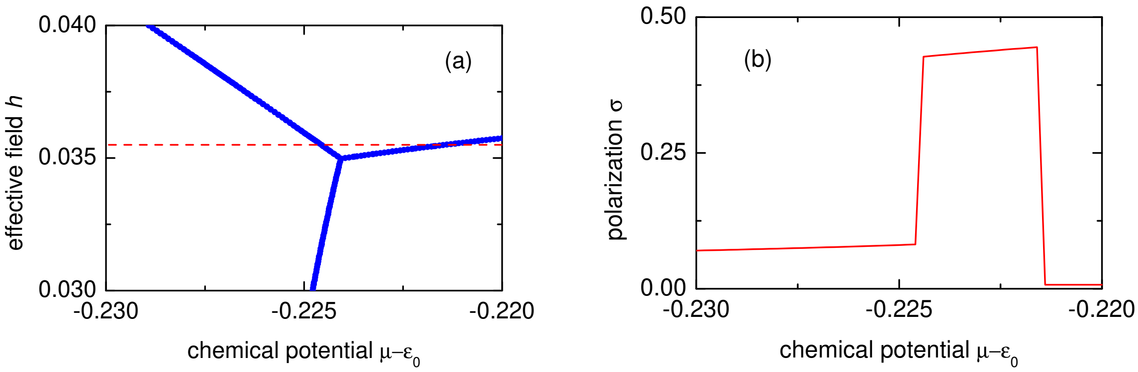

Figure 8. The temperature deformation of the phase diagram (a) allowing the jump-like behaviour of the polarization (b) due to the passing through three states at change of chemical potential (a dashed line in diagram (a)) at $\Theta = 0.19$, $\Delta = -0.03$, $V = 0.8$, $J = 0.2$, $U = 0.2$.

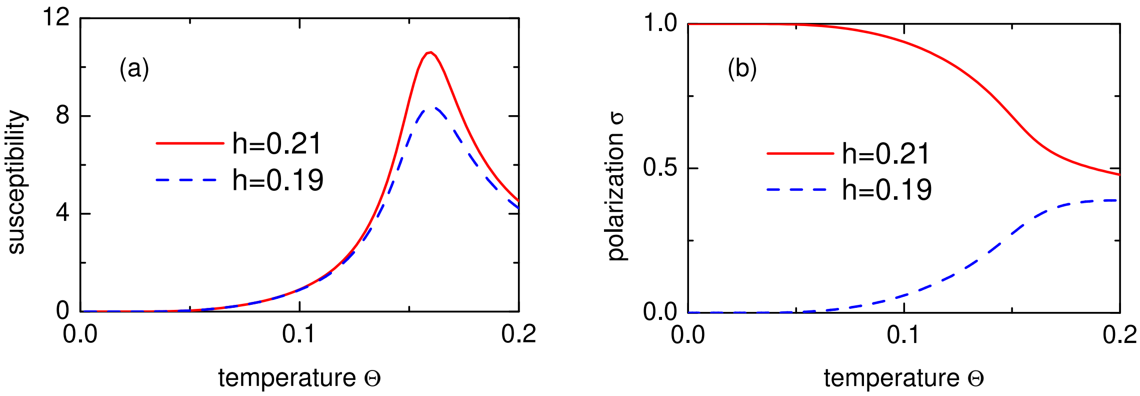

Figure 9. Temperature dependences of the susceptibility $\tilde{\chi}$ (a) and the polarization (b) starting from the polar ($h = 0.21$) and the non-polar ($h = 0.19$) occupied phases at $\mu = -0.4$, $\Delta = -0.1$, $V = 0.8$, $J = 0.7$, $U = 0.2$.

The estimated value of interaction energies is around $V + J = 0.2$ eV (so the dimensionless temperature $T = 0.1$ corresponds to about 200 K). Taking the value of the dipole moment as $d = 0.5$ Å $\cdot 2 \cdot 1.6 \cdot 10^{-19}$ C ≈ 5 D, we can assess the strength of the effective field $E = (V + J)h/d$; the dimensionless value $h = 0.01$ in figure 8(a) corresponds to $E = 20$ MV/m. If we assume that the electret voltage is proportional to the spontaneous polarization value and the intercalant concentration changes linearly with chemical potential, the jumps of the polarization (figure 8(b)) closely resemble the previously demonstrated peak behaviour of voltage at the change of concentration (figure 3). Dimensionless polarization σ is related to the real polarization as $P = (d/v_c)\sigma = 0.23\sigma$ (C/m^2), where $v_c = 7 \cdot 10^{-29}$ m^3 is the volume per formula unit.

The standard definition of transverse dielectric susceptibility is $\chi_\perp = \partial P/\partial E$; our results are presented for the susceptibility $\tilde{\chi}_\perp = \partial\sigma/\partial h$ related to the true one as

$$\chi_\perp = \frac{d^2}{\varepsilon_0 v_c (V + J)} \tilde{\chi}_\perp \approx 15\tilde{\chi}_\perp,$$

where ε_0 is the electric permittivity of vacuum. Temperature dependences of dielectric susceptibility demonstrate peaks (figure 9(a)) when the system passes near the lines of critical points. This behaviour again closely resembles the previously presented results of the dielectric permittivity measurements (figure 5). Peaks of susceptibility appear in cases when we start from both the polar phase “2” and the nonpolar phase “3” (figure 9(b)).

4. Conclusions

Measurements of dielectric properties of Ni intercalated GaSe and InSe revealed a pronounced unusual behaviour at small dopant concentrations ($x = 10^{-3} - 10^{-2}$). Namely, the electret effect and dielectric susceptibility demonstrate well-defined single peaks in this region. The temperature dependences of electret voltage exhibit a complex non-monotonous behaviour with the maximum values at low temperatures. A similar multi-peak behaviour is observed for dielectric permittivity of the GaSe crystal while for the InSe crystal a single-peak curve is obtained. For both the crystals these peaks diminish at the increase of concentration. Intercalation also leads to the increase of dielectric permittivity over the whole measured frequency range which is more pronounced at low temperatures. Especially profound growth (up to several orders) of the permittivity magnitude is observed at low frequencies.

The microscopic mechanism of the electret effect is presumably connected with redistribution of Ni cations between octahedral and tetrahedral positions causing the formation and ordering of quasi-dipoles in the crystals. The internal field stabilizing the ordered phase appears in the system due to redistribution and "freezing" of intrinsic impurities and charges. Based on these considerations, the order-disorder four-state model correctly describes the main features of the system thermodynamics. For instance, the calculated dependence of crystal polarization on chemical potential demonstrates a peak-like form due to the passing through the polar phase as intermediate one. Such a behaviour qualitatively coincides with the measured concentration dependences of the electret effect magnitude. The model also correctly predicts the existence of the peaks on temperature dependences of susceptibility (permittivity) in the vicinity of the line of critical points.

InSe and GaSe are semiconductors, so the intercalation process significantly effects their electron spectrums. Hence, an adequate theoretical model should take into account the electron subsystem of the compound. This task could be solved in future by extending the proposed model (similarly to the case of the $S = 1$ pseudospin-electron model [34]).

References

1. Medvedyeva Z.S., Chalcogenides of Subgroup IIIb of the Periodic Table. "Nauka" Publ., Moscow, 1968 (in Russian).
2. Man L.I., Imamov R.M., Semiletov S.A., Kristallografiya, 1976, **21**, 628 (in Russian).
3. Kuhn A., Chevy A., Chevalier R., Phys. Status Solidi A, 1975, **31**, 469.
4. Chevy A., Kuhn A., Martin M.S., J. Cryst. Growth, 1977, **38**, No. 1, 118.
5. Segura A, Guedson J.P., Besson J.M., Chevy A., J. Appl. Phys., 1982, **54**, 876.
6. Brandt N.B., Kulbachinskii V.A., Kovalyuk Z.D., Sov. Phys. Semicond., 1988, **22**, 720 (in Russian).
7. Grygorchak I.I., Kovalyuk Z.D., Mintyanskii I.V., Sov. Phys. Solid State, 1989, **31**, No. 2, 222 (in Russian).
8. Grigorchak I.I., Netyaga V.V., Kovalyuk Z.D., J. Phys.: Condens. Matter, 1997, **9**, L191.
9. Grigorchak I.I., Gavrylyuk S.V., Netyaga V.V., Kovalyuk Z.D., J. Phys. Studies, 2000, **4**, 82 (in Ukrainian).
10. Kulbachinskii V.A., Kovalyuk M.Z., Pyrlya M.N., J. Phys. I France, 1994, **4**, 975.
11. Schlüter M., Nuovo Cimento B, 1973, **13**, 313.
12. McCanny J.V., Murray R.B., J. Phys. C, 1977, **10**, 1211.
13. Robertson J., J. Phys. C, 1979, **12**, 4777.
14. Doni E., Girlanda R., Grasso V., Balzaroti A., Piacentini M., Nuovo Cimento B, 1979, **51**, 154.
15. Kunc K., Zeyher R., Europhys. Letters, 1988, **7**, 611.
16. Gomes da Costa P., Balkanski M., Wallis R.F., Phys. Rev. B, 1991, **43**, 7066.
17. Balkanski M., Gomes da Costa P., Wallis R.F., Phys. Status Solidi B, 1996, **194**, 175.
18. Rushchanskii K.Z., Sov. Phys. Solid State, 2004, **46**, No. 1, 177 (in Russian).
19. Berlinsky A.J., Unruh W.G., McKinnon W.R., Haering R.R., Solid State Commun., 1979, **31**, 135.
20. Lukyanyuk V.K., Kovalyuk Z.D., Phys. Status Solidi B, 1987, **102**, No. 1, K1.
21. Vakarin E.V., Filippov A.E., Badiali J.P., Phys. Rev. Lett., 1998, **81**, 3904.
22. Vakarin E.V., Badiali J.P., Levi M.D., Aurbach D., Phys. Rev. B, 2000, **63**, 014304.
23. Vakarin E.V., Badiali J.P., Solid State Ionics, 2004, **171**, No. 3–4, 261.
24. McKinnon W.R., Haering R.R. Physical mechanisms of intercalation. – In: Mod. Aspects Electrochem., **15**, Acad. Press, New-York, London, 1983, 235–261.
25. Stasyuk I.V., Tovstyuk K.D., Gera O.B., Velychko O.V. Preprint of the Institute for Condensed Matter Physics, ICMP–02–09U, Lviv, 2002 (in Ukrainian).
26. Grygorchak I.I., Kovalyuk Z.D., Tovstyuk K.D., Shastal M.M., USSR Patent No. 3326865 (9 November 1982) (in Russian).
27. Grygorchak I.I., Kovalyuk Z.D., Mintyanskii I.V., Tovstyuk K.D., USSR Patent No. 3630196 (1 April 1985) (in Russian).
28. Grygorchak I.I., Kovalyuk Z.D., Rybaylo V.O., Tovstyuk K.D., USSR Patent No. 4072673 (8 March 1988) (in Russian).
29. Mintyanskii I.V., Grygorchak I.I., Kovalyuk Z.D., Gavrylyuk S.V., Sov. Phys. Solid State, 1986, **28**, No. 4, 1263 (in Russian).
30. Tareyev B.M., Physics of Dielectric Materials. "Energiya" Publ., Moscow, 1973 (in Russian).

31. Zhukovskii P., Partyka Ya., Vengerek P., Shostak Yu., Sidorenko Yu., Rodzik A., Fiz. Tehnolog. Poluprovodnikov, 2000, **34**, No. 10, 1174 (in Russian).
32. Blume M., Emery V.J., Griffiths R.B., Phys. Rev. A, 1971, **4**, 1071.
33. Mukamel D., Krinsky S., Phys. Rev. B, 1975, **12**, 211.
34. Stasyuk I.V., Dublenych Yu.I., Phys. Rev. B, 2005, **72**, 224209.

Електретний ефект в інтеркальованих кристалах групи $A^{III}B^{VI}$

І.Григорчак[1], С.Войтович[1], І.Стасюк[2], О.Величко[2], О.Менчишин[2]

[1] Національний університет “Львівська Політехніка”, 79013 Львів, вул. С. Бандери, 12
[2] Інститут фізики конденсованих систем НАН України, 79011 Львів, вул. І. Свєнціцького, 1

Отримано 25 січня 2007 р.

Проведено вимірювання діелектричних властивостей GaSe та InSe, інтеркальованих Ni. Дана робота спрямована на дослідження в області низьких концентрацій домішки, де існує породжений інтеркаляцією електретний ефект. Для нього характерні виражені пікоподібні залежності від концентрації та немонотонна поведінка при зміні температури, де максимальні амплітуди досягаються для її низьких значень. Інтеркаляція приводить до понад десятикратного зростання діелектричної проникливості у всьому виміряному частотному діапазоні, а при низьких частотах для GaSe – збільшення на кілька порядків. Температурні залежності проникливості демонструють виразні піки, розташування та висота яких сильно залежать від концентрації. Запропоновано мікроскопічну модель типу лад-безлад, що враховує перерозподіл атомів інтеркалянта між неполярними октаедричними та полярними тетраедричними позиціями у ван-дер-ваальсових щілинах кристалів. Такий перерозподіл може відбутися у формі фазового переходу до полярної фази (що відповідає електретному ефекту), яка стабілізується внутрішнім полем. Для випадку, коли октаедричні позиції більш вигідні, модель передбачає пікоподібну залежність поляризації кристалів від хімічного потенціалу, спричинену проходженням через проміжну полярну фазу, що узгоджується з виміряною поведінкою електретного ефекту. Розраховані температурні залежності діелектричної сприйнятливості теж якісно відтворюють експериментальні результати для проникливості.

Ключові слова: *монохалькогеніди, електрети, інтеркаляція, модель типу граткового газу*

PACS: *71.20.Tx, 77.22.Ej, 71.10.-w, 05.50.+q*